Acta Pharmaceutica Sinica B xxxx;xxx(xxx):xxx

Chinese Pharmaceutical Association
Institute of Materia Medica, Chinese Academy of Medical Sciences

Acta Pharmaceutica Sinica B

www.elsevier.com/locate/apsb
www.sciencedirect.com

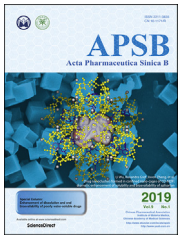

ORIGINAL ARTICLE

A nanocleaner specifically penetrates the blood–brain barrier at lesions to clean toxic proteins and regulate inflammation in Alzheimer's disease

Ting Lei[a], Zhihang Yang[a], Xue Xia[a], Yuxiu Chen[a], Xiaotong Yang[a], Rou Xie[a], Fan Tong[a], Xiaolin Wang[b], Huile Gao[a,*]

[a]*Key Laboratory of Drug–Targeting and Drug Delivery System of the Education Ministry and Sichuan Province, Sichuan Engineering Laboratory for Plant–Sourced Drug and Sichuan Research Center for Drug Precision Industrial Technology, West China School of Pharmacy, Sichuan University, Chengdu 610041, China*
[b]*School of Pharmacy and State Key Laboratory of Quality Research in Chinese Medicine, Macau University of Science and Technology, Macau 999078, China*

Received 21 February 2021; received in revised form 29 March 2021; accepted 30 March 2021

KEY WORDS

Alzheimer's disease;
Aβ capturing;
Autophagy;
ROS-responsive;
Anti-inflammatory;
blood–brain barrier transcytosis;
Microenvironment modulation;
Lesion targeting

Abstract Insurmountable blood–brain barrier (BBB) and complex pathological features are the key factors affecting the treatment of Alzheimer's disease (AD). Poor accumulation of drugs in lesion sites and undesired effectiveness of simply reducing Aβ deposition or TAU protein need to be resolved urgently. Herein, a nanocleaner is designed with a rapamycin-loaded ROS-responsive PLGA core and surface modification with KLVFF peptide and acid–cleavable DAG peptide [R@(ox-PLGA)-KcD]. DAG can enhance the targeting and internalization effect of nanocleaner towards neurovascular unit endothelial cells in AD lesions, and subsequently detach from nanocleaner in response to acidic microenvironment of endosomes to promote the transcytosis of nanocleaner from endothelial cells into brain parenchyma. Then exposed KLVFF can capture and carry Aβ to microglia, attenuating Aβ-induced neurotoxicity. Strikingly, rapamycin, an autophagy promoter, is rapidly liberated from nanocleaner in the high ROS level of lesions to improve Aβ degradation and normalize inflammatory condition. This design altogether accelerates Aβ degradation and alleviates oxidative stress and excessive inflammatory response. Collectively, our finding offers a strategy to target the AD lesions precisely and multi-pronged therapies for clearing the toxic proteins and modulating lesion microenvironment, to achieve efficient AD therapy.

*Corresponding author. Tel./fax: +86 18780288069.
E-mail addresses: gaohuile@scu.edu.cn, gaohuilescu@163.com (Huile Gao).

Peer review under responsibility of Chinese Pharmaceutical Association and Institute of Materia Medica, Chinese Academy of Medical Sciences.

https://doi.org/10.1016/j.apsb.2021.04.022

Please cite this article as: Lei Ting et al., A nanocleaner specifically penetrates the blood–brain barrier at lesions to clean toxic proteins and regulate inflammation in Alzheimer's disease, Acta Pharmaceutica Sinica B, https://doi.org/10.1016/j.apsb.2021.04.022

1. Introduction

Alzheimer's disease (AD) is the most common progressive neurodegenerative disease all over the world[1,2]. The immensely destructive nature of this disease and the increasing number of patients have pushed many researchers to look for efficient treatments.

Currently, marketed drugs are only a cure for the symptoms, not the causes, coupled with the insurmountable gastrointestinal side effects and poor drug delivery efficiency, which vigorously impair their therapeutic effect[3−6]. Besides, some new strategies, such as reducing amyloid deposits or interfering with the formation of neurofibrillary tangles, have been plagued by seemingly endless clinical trial failures[7,8]. Tracing its root, the pathological features of AD in addition to amyloid peptide aggregation and TAU phosphorylation[9,10], also include abnormal lesion microenvironment. The first to bear the brunt is the excessive activation of microglia. The autophagy lysosomal dysfunction in microglia directly affects the degradation of Aβ[11−13]. Meanwhile, overactive microglia release large amounts of ROS and inflammatory factors[14,15], causing oxidative stress and excessive inflammatory response, which not only promotes the spread of Aβ and TAU protein, but also greatly damages nerve cells[16,17]. The characteristics of AD were inter–connected, interacting and inter-prompting, forming an endless pathological cycle[18]. Consequently, a combinational therapeutic strategy is urgently needed.

Overwhelming evidence supports extracellular Aβ deposition and a cascade of events induced by it ultimately lead to neuronal damage and necrosis, wherefore the clearance of Aβ remains the top priority in the treatment of AD. Some studies utilized the good affinity of KLVFF and Aβ and modified it on the nanoparticles to capture and bring Aβ into the microglia to reduce extracellular Aβ deposition[19−21]. However, due to the dysfunctional autophagy-lysosome system of microglia cells in AD lesions, the effect was not good. And some researchers suggested that Aβ can be degraded by promoting autophagy[22,23], but the Aβ usually aggregates and deposits outside the cell while autophagic degradation occurs intracellularly, the conceive of cleaning Aβ only by improving autophagy is controversial. Thus, it is necessary to co-delivery KLVFF peptide with autophagy promoter. Rapamycin, as a specific inhibitor of mammalian rapamycin target protein (mTOR), has been shown to be effective against neurodegenerative diseases. (1) It can enhance cell autophagy to promote the degradation of Aβ and phosphorylated TAU protein. (2) It can regulate the level of β-secretase, γ-secretase and cAMP-dependent protein kinases to decrease the production of Aβ and phosphorylated TAU protein. (3) It can inhibit the synthesis of nitric oxide to reduce the level of inflammation and ROS in the AD lesions, and protect the survival and plasticity of nerve cells[24,25]. Therefore, we envisage to co-delivery KLVFF peptide and rapamycin to lesions. First KLVFF and rapamycin can synergistically complete the degradation of Aβ and second rapamycin can remodel the lesion microenvironment. In order to realize more accurate release and avoid multifunctional regulation of rapamycin from interfering with the cell behavior of other normal tissues, we designed an ROS-responsive release system based on the high level of ROS in the lesion. In this way, we can achieve a combination therapy system with precise drug release.

As a brain disease, the successful delivery of drugs to the lesion is also vital important. In previous studies, nonspecific blood–brain barrier (BBB) targeting peptides were commonly used in AD delivery systems[26,27]. These regimens usually indiscriminately target the BBB causing a relatively widespread distribution in the brain and poor accumulation of drugs in the lesions. The subsequent cascade targeting strategies did not greatly improve this problem[28−33]. Latterly, as cyclic peptide, CDAGRKQKC (designated as DAG), could specifically home to neurovascular unit endothelial cells and reactive astrocytes in AD lesions by targeting its receptor connective tissue growth factor (CTGF)[34]. Although the DAG could help nanoparticles directly target BBB in AD lesions, the difficulty in escaping lysosomes caused by the binding of ligand to receptor remains a non-negligible problem, which will affect the penetration of nanoparticles into brain parenchyma[35]. According to our previous experience, the design of an acid-cleavable target can promote the penetration of BBB[36], we therefore creatively linked DAG to an acid sensitive fragment to achieve specific penetration of BBB in AD lesions.

Herein, we designed a versatile nanocleaner integrating AD lesions specific targeting, Aβ capturing, stimuli-responsive drug release for cleaning extracellular Aβ and modulating lesion environment. The nanocleaner was composed of an ROS-responsive PLGA core loaded with rapamycin and decorated with KLVFF and DAG peptides [R@(ox-PLGA)-KcD] (Fig. 1). Under the guidance of DAG peptide, R@(ox-PLGA)-KcD first targeted to neurovascular unit endothelial cells and reactive astrocytes surround Aβ deposits. Then R@(ox-PLGA)-KcD underwent an acid-responsive cleavage of DAG, making the remainder of nanocleaner [R@(ox-PLGA)-K] further be exocytosed into brain parenchyma. Next, KLVFF–modified nanocleaner [R@(ox-PLGA)-K] recognized and co-assembled with Aβ to capture and carry it into microglial cells. Upon exposure to high ROS level in lesions, entrapped rapamycin could be readily released from the unconsolidated nanocleaner to promote autophagy and regulate microenvironment. Results from *in vitro* and *in vivo* experiments confirmed the Aβ clearance and microenvironment coordination efficiency of the nanocleaner. Furthermore, two AD animal models showed excellent therapeutic effects. This multi-pronged nano-strategy exhibited desirable therapeutic potential of AD.

2. Materials and methods

2.1. Materials

Inositol was purchased from Shanghai Yi En Chemical Technology Co., Ltd. (Shanghai, China). Oxalyl chloride and Thioflavin-T

Please cite this article as: Lei Ting et al., A nanocleaner specifically penetrates the blood–brain barrier at lesions to clean toxic proteins and regulate inflammation in Alzheimer's disease, Acta Pharmaceutica Sinica B, https://doi.org/10.1016/j.apsb.2021.04.022

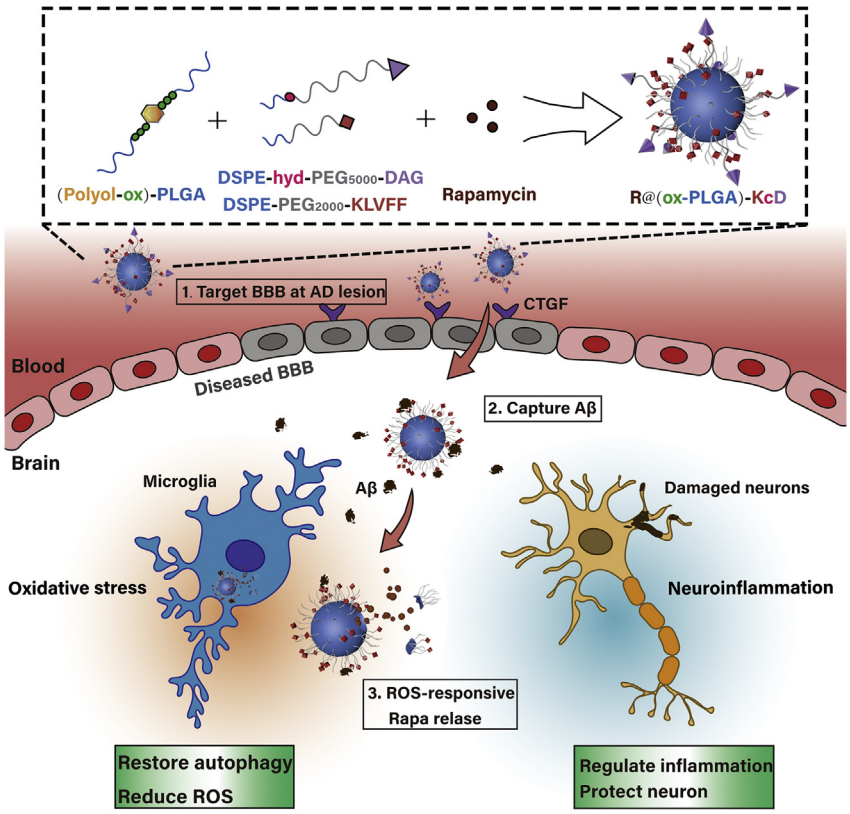

Figure 1 Scheme of the ROS–responsive specific targeted R@(ox–PLGA)–KcD.

was obtained from Sigma−Aldrich Co., LLC (USA). DSPE-PEG_{2000}-Mal and DSPE-PEG_{5000}-Mal were purchased from Ponsure Biotechnology (Shanghai, China). DSPE-hyd-$DSPE_{5000}$-Mal was obtained from Jenkem Technology Co., Ltd. (Beijing, China). PLGA (MW = 3000) was gained from Trueturn-Biological technology Co., Ltd. (Beijing, China). The KLVFFC and C-Acp-Cyclo (CDAGRKQKC) were synthesized by Sangon Biotech Co., Ltd. (Shanghai, China). $A\beta_{1-42}$ and $A\beta_{42}$-FITC were obtained from GL Biochem Ltd. (Shanghai, China). Rapamycin was purchased from Dalian Meilun Biotech Co., Ltd. (Dalian, China). 4-Chlorobenzenesulfonate salt (DiD) was gained from Biotium (Hayward, CA, USA). The anti-TAU (phospho S396) and anti-beta $amyloid_{1-42}$ were purchased from Abcam Ltd. (Cambridge, UK), and the APP polyclonal antibody and phosphorylated TAU antibody [p-TAU (Ser 404)] were purchased from Abclonal (China). ELISA kits (IL-10, IFN-γ and TNF-α) was obtained from BD Pharmingen (USA). Tissue ROS test kit were purchased from BestBio Science (Nanjing, China). The chemical used in this study were analytical grade.

2.2. *Cell lines and animals*

The human glioblastoma astrocytoma cells (U251) and the nerve growth factor-differentiated rat pheochromocytoma cells (PC12) were obtained from the Chinese Academy of Sciences Cell Bank (Shanghai, China). Male BALB/c mice were derived from Dashuo Biotechnology Co., Ltd. Male C57BL/6 were purchased from Byrness Weil Biotech Ltd. (Chongqing, China). B6-Tg (APPswePSEN1DE9) mice were derived from the Nanjing Biomedical Research Institute of Nanjing University (Nanjing, China). All animals were raised under standard living conditions. All animal experiments were conducted in accordance with the guidelines approved by the Experimental Animal Management Committee of Sichuan University, China.

2.3. *Synthesis of core nanoparticles [(Polyol-ox)-PLGA]*

(Polyol-ox)-PLGA was obtained *via* acylation reaction in two steps: (1) the inter-mediate product Polyol–ox was obtained by acylation of oxalyl chloride with inositol; (2) the (Polyol-ox)-PLGA was obtained by acylation of Polyol-ox with PLGA (MW = 3000). Briefly, 0.25 g inositol (1.4 mmol/L) was dissolved in 4 mL anhydrous THF under the protection of argon and stirred at 30 °C for 30 min. Following 0.93 mL oxalyl chloride (11 mmol/L) was dripped slowly into the reaction system at room temperature. Then, the mixture was stirred constantly at 30 °C for 20 h. After the reaction, solvent THF was removed by rotary evaporation, and the product was further dried by vacuuming. The obtained intermediate product Polyol–ox showed a pale yellow foamy solid. After that, 150 mg PLGA (0.05 mmol/L) and 5.42 mg Polyol-ox (0.01 mmol/L) were dissolved in 3 mL anhydrous THF. The mixture was stirred for 48 h at room temperature under the protection of argon. After the reaction completed, the resulting solution was dried by a rotary evaporator and then was recrystallized with good solvent chloroform and bad solvent methanol for further separation and purification.

2.4. *Thioflavin-T assay*

The concentrated solution of Thioflavin T (ThT 0.7 mg/mL) and $A\beta_{1-42}$ (1 mg/mL) were firstly prepared. Then the ThT and $A\beta_{1-42}$ were both diluted to a final concentration of 20 μmol/L

Please cite this article as: Lei Ting et al., A nanocleaner specifically penetrates the blood–brain barrier at lesions to clean toxic proteins and regulate inflammation in Alzheimer's disease, Acta Pharmaceutica Sinica B, https://doi.org/10.1016/j.apsb.2021.04.022

into glycine/NaOH (90 mmol/L, pH 8.5). Following, this mixture was added to the 96–well plate at 100 μL per well, and incubated with different samples: ox-PLGA, (ox-PLGA)-K, (ox-PLGA)-KD and KLVFF. The molar ratio of Aβ_{1-42}/samples was 1/2. Three replicates were made for each sample and then averaged the results. After incubation at 37 °C for 24 h, the ThT fluorescence in plates was tested with an excitation wavelength of 450 nm and emission at 485 nm by microplate reader.

2.5. Anti-Aβ toxicity assay

Firstly, PC-12 cells were inoculated on 96-well plate (1×10^4 cells/per well). After the cells have grown for 24 h, the original medium was removed, and then added fresh medium (control) or medium containing Aβ (10 μmol/L). Next, different concentrations of ox–PLGA, (ox-PLGA)-K, (ox-PLGA)-KD, KLVFF, and PBS were added into corresponding wells. The ratio of each nanoparticle to Aβ was set with different molar ratios, which are 1−5, 1−10, and 1−20, respectively. 24 h later, the prepared MTT solution (5 mg/mL) was given to each well (10 μL per well). Finally, the absorbance at 570 nm was detected by microplate reader after incubating with MTT solution for 4 h.

2.6. Cell targeting experiment

The U251 cells were inoculated into 6-well plate (5×10^5 cells per well). After grown for 24 h, the cells were treated with different nanoparticles labeled with coumarin-6.3 h later, the cells were stained with DAPI (0.5 μg/mL) for 5 min. Then the laser scanning confocal microscopy (A1R+, Nikon, Japan) was employed to observe the co-localization of nanoparticles with cells.

The PC-12 cells and BV-2 cells were inoculated in 6–well plate (3×10^5 cells per well). After grown for 24 h, the Aβ (Aβ–FITC/Aβ = 1/10) and different nanoparticles were added into the 6-well plate. After 3 h incubation, culture medium was removed, and the cells were washed three times with PBS. Finally, cells were digested and collected for testing by flow cytometry (Becton, Dickinson and Company, USA).

2.7. In vitro BBB transcytosis

The U251 cells were inoculated under the chambers of Transwells (24-well; pore size: 3 μm; Corning, USA) (1×10^6 cells per well). After U251 cells adherence, the bEnd.3 cells were inoculated into inserts (1×10^5 cells per well), so that the endothelial cell line could contact with the glioblastoma astrocytoma cells through the micropores[37]. The culture medium was replaced every 1−2 days. The integrity of this bilayer was monitored using transendothelial electrical resistance (TEER) measurements (Millicell-ERS, Millipore, USA). After the transmembrane resistance of the model reached 200 Ω, added new medium containing Aβ (5 μmol/L) into corresponding wells. After 24 h, replaced the medium and added different nanoparticles labeled with coumarin-6 into the chambers of Transwells. 4 h later, the confocal microscope was used to observe the imaging of this bilayer.

2.8. In vivo imaging

Firstly, AD model was established by injecting Aβ_{1-42} into hippocampus according to the method described previously[38]. The male mice were anesthetized and fixed in a stereotactic device. Aβ_{1-42} was dissolved in artificial cerebrospinal fluid (1 mg/mL) and pre-incubated at 37 °C for 7 days. Next, Aβ_{1-42} (5 μL) was injected into the right hippocampus for 8 min and then withdrawn slowly. Two weeks after the operation, the mice were intravenously injected with the DiD-labeled nanoparticles and imaged by the Lumina III Imaging System (PerkinElmer, USA) at 2, 4, 8, 12, 24, 36 and 48 h post injection. At the same time, some mice were executed at the 8 h, and then their major organs were separated for *ex vivo* imaging. The fluorescence of the organs was measured as above. Next, the tissues were sectioned after the fixation and dehydration steps by freezing microtome (Leica CM1950, Germany). At last, the tissues were stained with DAPI (1 μg/mL). The images were observed using a confocal microscope.

2.9. Behavioral experiment

Morris water maze (MWM): MWM were used to evaluate the spatial cognitive performance. Whether the dosage or frequency of administration, the same treatment was used in two AD models (8-month-old APPswe/PSEN1DE9 transgenic mice and Aβ-injected mice). Here, Aβ-injected mice model provided an example. The Aβ-injected mice were randomly divided into 4 groups ($n = 11$) and gave appropriate medication. Healthy mice were performed sham operation for reducing the error caused by the surgery. High dose (0.7 mg/kg), low dose (0.35 mg/kg) of R@(ox-PLGA)-KcD, free rapamycin (0.7 mg/kg) and PBS were administered intravenously once every two days. After giving 7 treatments, the mice were performed MWM test. Firstly. A 4-days behavior training were conducted before the test. The mice were placed in a white round pool (100 cm in diameter). There was a circular platform in the water, which was about 1 cm away from the water surface. If the mice find the platform within 60 s and stay for at least 10 s, it is considered a successful training. If not, they will be artificially guided to the platform and stay for 10 s. On the fifth day, the platform was removed and the spatial probe test was performed. The mice were allowed to swim freely for 60 s. The latency to reach the platform, average frequencies across original platform location and cumulative time at original platform location were recorded for statistical analysis.

Y-maze: To further study short-time memory ability, the AD mice were measured by Y-maze. It had three arms (A, B, C arms) of the same size (30 cm long, 8 cm wide and 15 cm height). The angle between the arms was 120°. We put the mice in one arm (A arm), and then recorded the sequence of mice entering each arm in 480 s. Pre-training was conducted to familiarize mice with Y-maze.

2.10. Mechanism experiments after treatment

After the treatment, we collected blood from the eyes of the mice before the execution. After the blood was allowed to stand for 2 h, the supernatant was separated by centrifugation to obtain serum, and the inflammatory factors in the serum were measured by ELISA Kit. Next, the major organs were separated. The cross sections of the hippocampus of some brains were selected for staining. The hippocampal tissues in some brains were homogenized by a high-speed tissue grinder (Servicebio, Wuhan, China) to perform Western blot, ELISA assay and ROS experiments, respectively.

2.11. Evaluation of systemic toxicity

During the treatment, all mice were weighed once every three days. The weight changes of each group were counted after

Please cite this article as: Lei Ting et al., A nanocleaner specifically penetrates the blood–brain barrier at lesions to clean toxic proteins and regulate inflammation in Alzheimer's disease, Acta Pharmaceutica Sinica B, https://doi.org/10.1016/j.apsb.2021.04.022

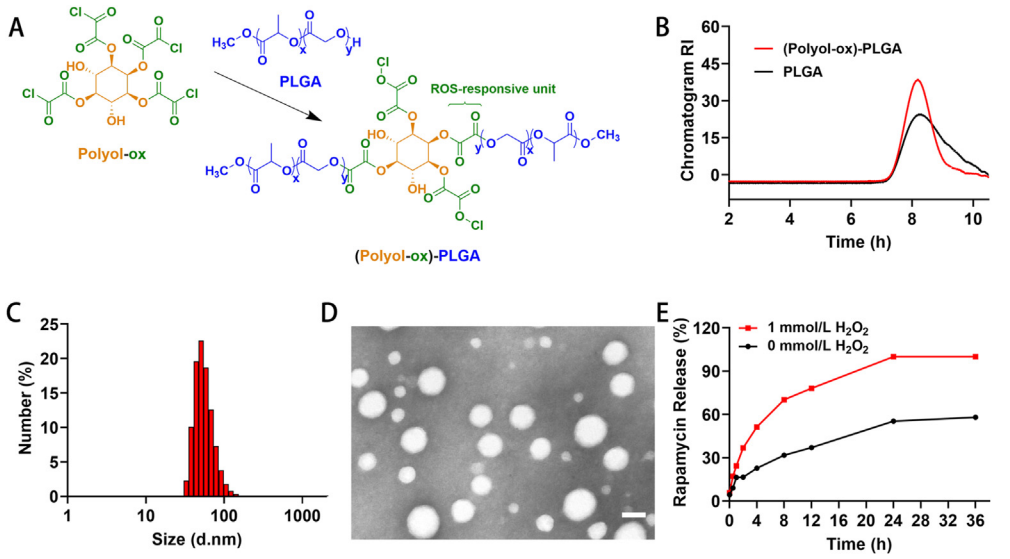

Figure 2 Synthesis and characterization of the R@(ox-PLGA)-KcD. (A) Synthesis scheme of (Polyol-ox)-PLGA. (B) GPC analysis of (Polyol-ox)-PLGA. (C) DLS analysis of R@(ox-PLGA)-KcD. (D) TEM image of R@(ox-PLGA)-KcD in PBS. Scale bar = 50 nm. (D) Cumulative release rate of R@(ox-PLGA)-KcD in PBS with 0 mmol/L and 1 mmol/L H_2O_2. Data are presented as mean ± SD (n = 3).

administration. Meanwhile, H&E staining was used to observe the pathological changes of visceral sections of mice, so that the systemic cumulative toxicity of nanoparticles could be observed.

2.12. *Statistical analysis*

All data are presented as mean ± standard deviation (SD). Unpaired Student' s t-test was used for comparison of two groups.

3. Results

3.1. *Synthesis and characterization of R@(ox-PLGA)-KcD*

The intermediate product Polyol-ox with ROS sensitive bond was synthesized from inositol and oxalyl chloride, ^{1}HNMR and electrospray ionization mass spectrometry (ESI-MS) illustrated that it was successfully synthesized (Supporting Information Figs. S1A and S1B). Then one Polyol-ox was connected with two PLGA (MW = 3000) molecules to form two-arm nunchaku-shape biodegradable polymer (Polyol-ox)-PLGA (Fig. 2A), which was demonstrated by gel permeation chromatography (GPC) (Fig. 2B). KLVFFC (MW = 755.5) and C-Acp-Cyclo (CDAGRKQKC) (MW = 1222) were connected with DSPE-PEG_{2000}-Mal and DSPE-hyd–PEG_{5000}-Mal, respectively. From the matrix-assisted laser desorption/ionization time of flight mass spectrum (MALDI-TOF-MS) (Supporting Information Figs. S2A–S2D), the DSPE-PEG_{2000}-Mal peak at m/z about 2900 and the DSPE-hyd-PEG_{5000}-Mal peak at m/z about 5600 moved to about 3600 and 6800, respectively, indicating that DSPE-PEG_{2000}-KLVFF and DSPE-hyd-PEG_{5000}-DAG were successfully synthesized. In addition, we have also confirmed that the hydrazone bond in DSPE-hyd-PEG_{5000}-DAG would break under the acidic environment (Supporting Information Figs. S2E and S2F). On the contrary, the DSPE-PEG_{5000}-DAG without hydrazone bond didn't have such a phenomenon (Supporting Information Figs. S2G−S2J). Next, rapamycin was encapsulated into nanoparticles by Ultrasonic Homogenizer (SCIENTZ, JY92-IIN, Ningbo, China), and the most suitable particle size and zeta potential were obtained by optimizing the preparation methods. The number mean size of R@(ox-PLGA)-KcD was 60.0 ± 5.9 nm (Fig. 2C), and the zeta potential was −30.5 ± 1.4 mV, which were measured by the dynamic light scattering (DLS). Transmission electron microscopy (TEM) and showed that the nanoparticles were regular round with good uniformity (Fig. 2D).

To verify the stability of nanoparticles, nanoparticles were incubated with phosphate buffer solution (PBS), 10% and 50% fetal bovine serum (FBS), respectively (Supporting Information Fig. S3). Within 36 h, there was no significant increase in particle size or polydispersity index (PDI). Compared with PBS without H_2O_2, the release rate of rapamycin in PBS with 1 mmol/L H_2O_2 was obviously increased (Fig. 2E), indicating the drugs loaded in nanoparticles were released responsively. TEM showed that the structure of ROS-responsive nanoparticles [R@(ox-PLGA)-KcD] changed obviously after incubating with PBS containing H_2O_2 for 12 h, but no change was observed in PBS(Supporting Information Figs. S4A and S4B). In comparison, the structure of nanoparticles composed of PLGA without ROS bond modification (R@PLGA-KcD) didn't change observably before and after incubation (Supporting Information Figs. S4C and S4D). These results confirm that PLGA modified with Polyol-ox could make the nanoparticle respond to ROS to release the drugs quickly. Since the ROS level of normal tissues and cells remain relatively low, these features of nanoparticles can support the selective release of drugs in the pathological environment of AD.

3.2. *Evaluation of Aβ capturing and anti-Aβ toxicity*

First, we visually observed the role of nanoparticles in capturing Aβ through TEM imaging (Fig. 3A). Compared with simple (ox-PLGA)-K nanoparticles, after co-incubation with Aβ, a thin film was clearly observed on its outer surface, and a large number of fibers formed after simple Aβ incubation were not found, which indicated that Aβ co-incubated with nanoparticles modified with KLVFF could form nanoparticles/Aβ complex to inhibit the

Please cite this article as: Lei Ting et al., A nanocleaner specifically penetrates the blood–brain barrier at lesions to clean toxic proteins and regulate inflammation in Alzheimer's disease, Acta Pharmaceutica Sinica B, https://doi.org/10.1016/j.apsb.2021.04.022

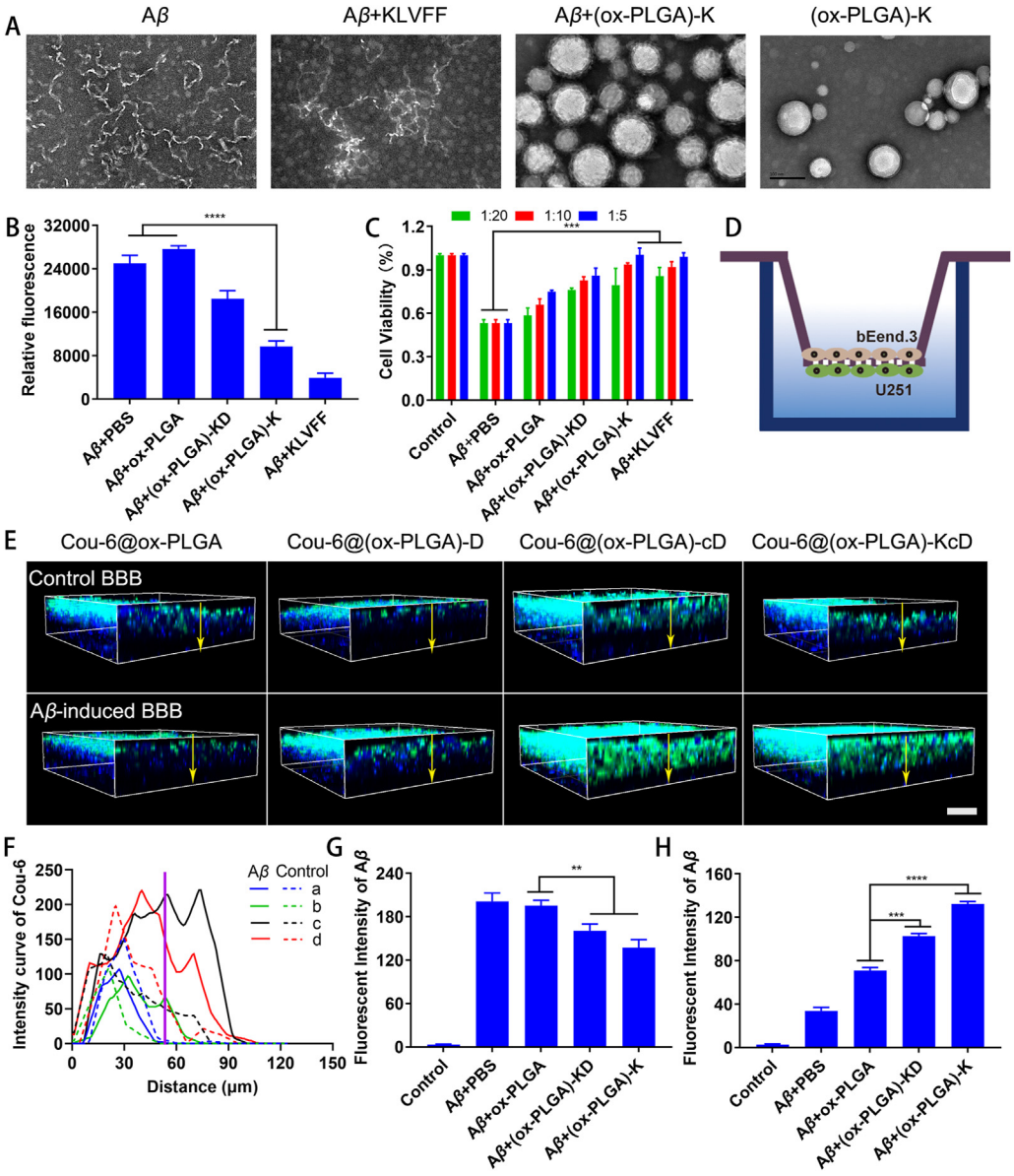

Figure 3 The anti-Aβ toxicity and targeting ability of nanoparticles. (A) TEM images of Aβ, Aβ/KLVFF, *Aβ*/(ox-PLGA)-K and (ox-PLGA)-K at 24 h. Scale bar = 100 nm. (B) The binding of nanoparticles to Aβ was showed by ThT assay after incubation monomeric Aβ_{1-42} with different nanoparticles for 24 h at 37 °C. Data are presented as mean ± SD (n = 3). ***$P < 0.001$. (C) The anti-Aβ toxicity of KLVFF, (ox-PLGA)-K, (ox-PLGA)-KD and ox-PLGA in PC-12 cells. The molar ratios of nanoparticle/Aβ were 1/5 (blue), 1/10 (red) and 1/20 (green), respectively. Data are presented as mean ± SD (n = 3). ***$P < 0.001$. (D) The schematic illustration of transwell model. (E) 3D confocal images of bEnd.3 and U251 contact co-cultured bilayer in the donor chamber of transwell model after the introduction of different formulations for 4 h. Scale bar = 40 μm. (F) Intensity curve of coumarin-6 at the indicative location and distance from E. a, Cou-6@ox-PLGA; b, Cou-6@(ox-PLGA)-D; c, Cou-6@(ox-PLGA)-cD; d, Cou-6@(ox-PLGA)-KcD. (G and H) Uptake of Aβ by PC-12 (G) and BV-2 cells (H) after treatment with different formulations. The concentration of Aβ was 5 μmol/L. Aβ was labeled with FITC (molar ratio of Aβ-FITC/Aβ was 1/10). Data are presented as mean ± SD (n = 3). **$P < 0.01$, ***$P < 0.001$, ****$P < 0.0001$.

aggregation of Aβ. Then we continued to study the binding efficiency of nanoparticles to Aβ by an established method of dye binding thioflavin T (ThT) fluorescence assay, which was used to detect the aggregation of Aβ due to its fluorescent spectrum changed with fiber growth[39]. Compared with the control group (PBS) and the nanoparticles without peptide modification group (ox-PLGA), the fluorescence intensity of ThT decreased significantly in the nanoparticles containing KLVFF peptide groups (Fig. 3B), indicating that the nanoparticles modified with KLVFF peptide had a good affinity with Aβ. Moreover, nanoparticles modified with only KLVFF peptide [(ox-PLGA)-K] had lower fluorescence intensity than those modified with KLVFF peptide and acid-uncleavable DAG peptide [(ox-PLGA)-KD]. The main reason was that DAG peptide was attached to a longer chain DSPE-PEG$_{5000}$, which had a certain extent protection and shielding effect on the KLVFF peptide inside. This also reflected

Please cite this article as: Lei Ting et al., A nanocleaner specifically penetrates the blood–brain barrier at lesions to clean toxic proteins and regulate inflammation in Alzheimer's disease, Acta Pharmaceutica Sinica B, https://doi.org/10.1016/j.apsb.2021.04.022

the necessity of acid-cleavable design, which was to avoid affecting the binding of KLVFF peptide to Aβ.

We then verified at the cellular level whether inhibiting the aggregation of Aβ can reduce the toxicity caused by Aβ. Firstly, we investigated the cytotoxicity of nanoparticles by methyl-thiazolyl-tetrazolium (MTT) assay. The murine pheochromocytoma cells PC-12 showed approximately 100% viability in different groups of nanoparticles at less than 20 μg/mL (Supporting Information Fig. S5A), indicating that the nanoparticles had good biocompatibility. Next, to investigate the anti–Aβ toxicity of nanoparticles, PC-12 cells were treated with Aβ (10 μmol/L) and different nanoparticles. As expected, compared with those treated with Aβ/PBS that had only half survival (53.4%), the cell viability increased significantly in those treated with nanoparticles containing KLVFF peptide. More optimistically, cell survival rate surpassed 100% after incubating with (ox-PLGA)-K/Aβ [the molar ratio of (ox-PLGA)-K/Aβ was 1/5] (Fig. 3C). These results altogether indicated the nanoparticles with KLVFF peptide could effectively reduce Aβ-induced toxicity by mean of capturing Aβ and forming nanoparticles/Aβ complex.

3.3. Nanoparticles targeting in vitro

The bEnd.3 cells and U251 cells were used to establish a normal BBB model *in vitro* by contact co-culture (Fig. 3D), which was more relevant to the real BBB environment than the commonly used monolayer model[40]. The transmembrane resistance of the model was measured every day until it reached 200 Ω. Then Aβ (5 μmol/L) was incubated with the model for 24 h to simulate the BBB at the AD lesions because the Aβ could activate astrocytes and stimulate CTGF receptor expression, which is the receptor of DAG[41]. The normal and AD-mimetic BBB models were incubated with different nanoparticles labeled with coumarin-6 for 4 h. The 3D confocal images of the model displayed that penetrability of nanoparticles containing acid-cleavable DAG peptide groups [Cou-6@(ox-PLGA)-cD and Cou-6@(ox-PLGA)-KcD] were significantly deeper than that of nanoparticles without peptide modification (Cou-6@ox-PLGA) and with acid–uncleavable DAG peptide modification [Cou-6@(ox-PLGA)-D] (Fig. 3E). From the fluorescence quantitative analysis, the intensity curve of coumarin-6-loaded nanoparticles with acid–cleavable DAG exhibited about two times longer extension than that of other formulations (Fig. 3F). But this phenomenon was not observed in normal BBB model without Aβ stimulation. These results demonstrated that nanoparticles with acid-cleavable DAG could specifically penetrate AD-mimetic BBB model. Then we explored the binding efficiency of nanoparticles to U251 cells by confocal imaging. Compared with nanoparticles without peptide modification, nanoparticles with DAG peptide bound more robustly to U251 cells. Meanwhile, this binding was specific, which was inhibited by co-incubation with free DAG peptides (Supporting Information Fig. S5B). All these finding further confirmed that the cleavable-DAG coating was beneficial for the specific brain targeting of nanoparticles as well as relatively more BBB penetration.

Subsequently, we studied the uptake of Aβ by PC-12 cells and BV-2 cells after co-incubation of nanoparticles with Aβ. For PC-12, the uptake rates of Aβ in the PBS group and the nanoparticles without peptide modification (ox-PLGA) group were higher than that of the nanoparticles with KLVFF peptide (Fig. 3G). The results implied that for ordinary neurons, nanoparticles with KLVFF peptide could capture Aβ and then reduced its uptake by neurons, which explained the neurotoxicity mediated by Aβ could be relieved by KLVFF modified nanoparticles. Studies showed that Aβ in the brain was usually cleared by microglia[42]. Therefore, murine microglial BV-2 was employed to evaluate the uptake of Aβ. Surprisingly, we got an opposite result. The amount of Aβ in cells treated with (ox-PLGA)-K were 3.9–, 1.9– and 1.3–fold higher than those treated with PBS, ox-PLGA, and (ox-PLGA)-KD group, respectively (Fig. 3H). From this result, we found it was not easy for free Aβ to be endocytose by microglia, but after incubation with KLVFF modified nanoparticles, it was more prone to be internalized. Then we found that there was no significant difference in the uptake behavior of nanoparticles themselves in the two cells, which confirmed that the difference in the uptake of Aβ by the cells had nothing to do with the uptake behavior of the nanoparticles themselves. This mainly depended on the difference in the ability of the nanoparticles to capture Aβ, which would affect the amount of Aβ carried into the cell (Supporting Information Fig. S6). Combined with the ThT and TEM results, we can conclude that the nanoparticles can capture Aβ and form nanoparticles/Aβ complex, which reduced the uptake of Aβ by neurons and promoted the uptake by microglia, alleviating Aβ–mediated neurotoxicity and reducing the extracellular Aβ deposition.

3.4. In vivo targeting and distribution of nanoparticles

To evaluate the brain targeting efficiency of nanoparticles *in vivo*, we injected different nanoparticles labeled with DiD into AD mice (Aβ-injected mice) and monitored them with living fluorescent imaging (Fig. 4A). The nanoparticles with DAG peptide had significantly stronger intensity in brain than those without DAG peptide, validating the potent brain targeting capacity of DAG. Importantly, the fluorescence intensity of nanoparticles with acid-cleavable DAG was stronger than those with acid-uncleavable DAG, indicating the nanoparticles could penetrate the BBB more effectively after detaching cleavable DAG. At 8 h post injection, the major organs of AD mice were isolated for *ex vivo* imaging (Fig. 4B). As such, these DAG-coating nanoparticles all exhibited stronger fluorescence signal in the brain than DiD@ox-PLGA, especially those with acid–cleavable DAG groups. Furthermore, quantitative results displayed that the fluorescence intensity of brain in DiD@(ox-PLGA)-D, DiD@(ox-PLGA)-cD and DiD@(ox-PLGA)-KcD groups was 1.19, 1.32 and 1.76 times higher than that in DiD@ox-PLGA group, respectively (Fig. 4C). The results further proved the above-mentioned conclusion. Afterwards, the major tissues were sliced and observed by confocal fluorescence microscopy (Fig. 4D and Supporting Information Fig. S7), which was in accordance with the above results. These results altogether supported the nanoparticles modified with DAG peptide could achieve brain targeting, and cleavable DAG could facilitate the penetration of nanoparticles, which was consistent with the BBB penetration results.

3.5. Evaluation of the effect to rescue memory deficits

Morris water maze (MWM) and Y maze were used to evaluate the spatial cognitive performance and short–time memory ability, respectively. As a control group, healthy mice were performed sham operation for reducing the error caused by the surgery. After the treatment period, we first gave all mice four days of indistinguishable spatial learning training before the MWM test. The spatial learning and memory retention of the mice treated with R@(ox-PLGA)-KcD were significantly better than those treated

Please cite this article as: Lei Ting et al., A nanocleaner specifically penetrates the blood–brain barrier at lesions to clean toxic proteins and regulate inflammation in Alzheimer's disease, Acta Pharmaceutica Sinica B, https://doi.org/10.1016/j.apsb.2021.04.022

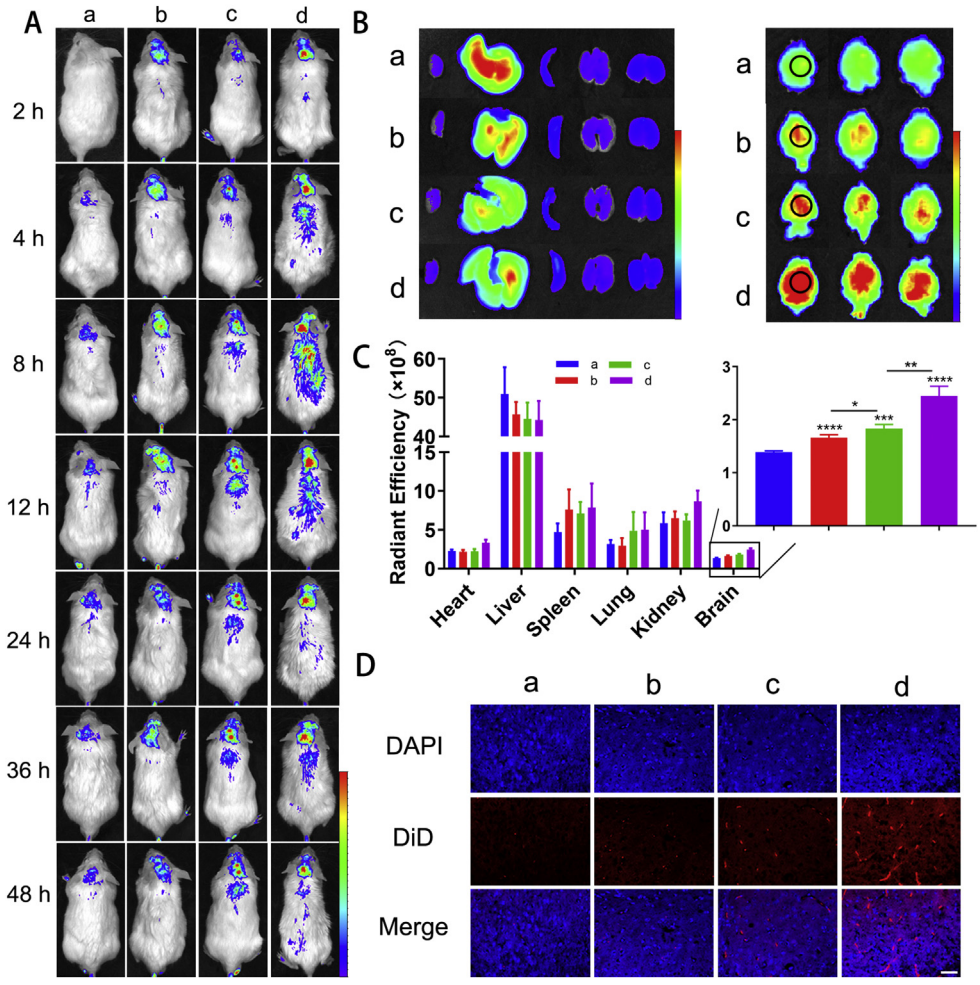

Figure 4 *In vivo* distribution. (A) Living imaging of AD mice (Aβ-injected mice) after intravenously injection with different formulations at different time–intervals. Bar represents radiant efficiency from 4.0×10^8 to 1.0×10^9 [p/s]/[μW/cm^2]. (B) *Ex vivo* imaging of tissues in each group after injection 8 h. Bar represents radiant efficiency from 2.0×10^8 to 8.0×10^9 and 4.0×10^7 to 2.5×10^8 [p/s]/[μW/cm^2], respectively. The black circle showed the area where Aβ was injected. (C) Semi–quantitative analysis of fluorescence intensity from B. Data are presented as mean ± SD ($n = 3$). *$P < 0.05$, **$P < 0.01$, ***$P < 0.001$, ****$P < 0.0001$. (D) Fluorescence distribution in brain slices after injection different formulations for 8 h a, DiD@ox-PLGA; b, DiD@(ox-PLGA)-D; c, DiD@(ox-PLGA)-cD; d, DiD@(ox-PLGA)-KcD. Scale bar = 50 μm.

with PBS or free rapamycin, both in low and high dosage. According to latency to reach the platform (Fig. 5A), the mice in PBS group took the longest time (52.4 ± 13.3 s), followed by the free rapamycin group (40.3 ± 17.2 s), while the mice of R@(ox-PLGA)-KcD groups both in low (15.5 ± 8.4 s) and high dose (14.4 ± 8.6 s) took about similar time as sham–operation group (13.4 ± 10.9 s). Meanwhile, other representative statistical results, for instance, average frequencies across original platform location and cumulative time at original platform location (Figs. 5B–5D and Supporting Information Figs. S8A and S8B), were also in accordance with above results. These outcomes were further confirmed on transgenic mice (Supporting Information Figs. S8C–S8E).

To further study the short–time memory ability of AD mice, we placed the mice in one of the arms of the Y maze, and then recorded the sequence of mice entering each arm in 480 s. Alternating defined as continuous access to three different arms was regarded as evaluation index of short–time memory ability. The alternating in low and high dose groups were both higher than AD group (Supporting Information Fig. S8F). The results of transgenic mice were agreed with the above (Supporting Information Fig. S8G). From two AD animal models and two behavioral experiments, it was fully demonstrated that R@(ox–PLGA)–KcD had significant therapeutic effects on rescuing memory deficits of AD mice.

3.6. *Evaluation of inducing autophagy and cleaning toxic protein in vivo*

In order to further explore therapeutic mechanism, we focused first on the autophagy regulation *in vivo*. After treatment, the total protein in the hippocampus of the transgenic mice brain was extracted. And then the Western blot was employed to observe the changes in levels of autophagy related proteins light chain 3-II (LC3-II) and P62. In the administration groups especially high dose group, the expression of LC3-II was increased and P62 was reduced, suggesting that autophagy levels have been raised after receiving R@(ox-PLGA)-KcD treatment. The enhanced autophagy was helpful to restore the ability to degrade toxic proteins, such as reducing Aβ levels and relieving TAU pathological

Please cite this article as: Lei Ting et al., A nanocleaner specifically penetrates the blood–brain barrier at lesions to clean toxic proteins and regulate inflammation in Alzheimer's disease, Acta Pharmaceutica Sinica B, https://doi.org/10.1016/j.apsb.2021.04.022

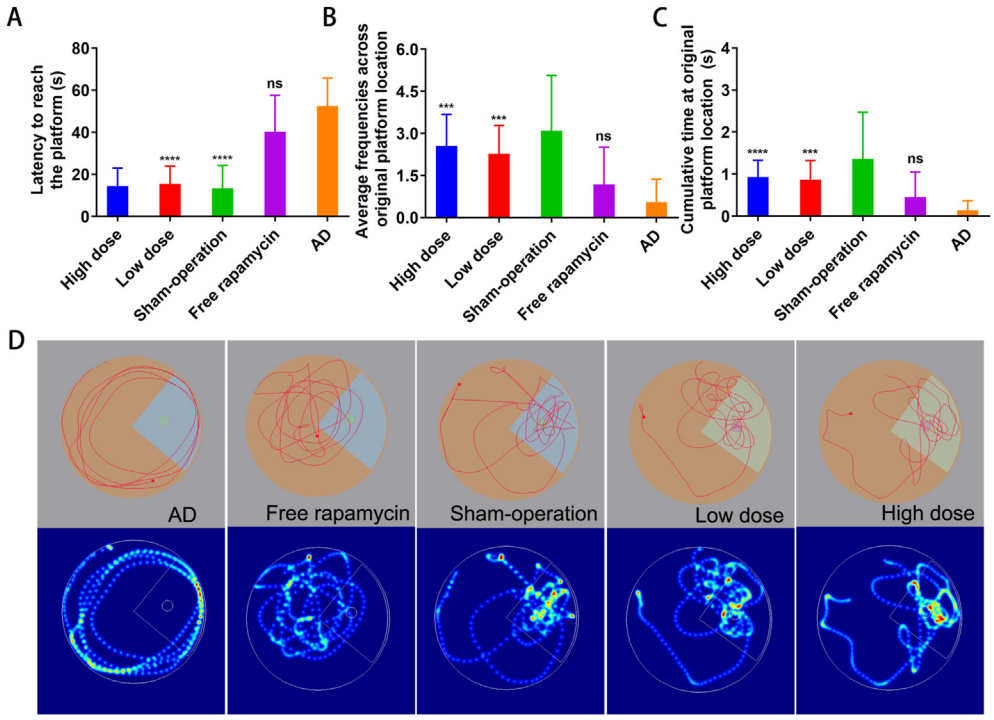

Figure 5 Behavioral experiment. (A) The time for mice to reach the platform. Data are presented as mean ± SD ($n = 11$). ****$P < 0.001$, n.s., not significant. (B) The average frequencies for mice to across original platform location. Data are presented as mean ± SD ($n = 11$). ***$P < 0.001$, n.s., not significant. (C) The cumulative time for mice to spent at original platform location. Data are presented as mean ± SD ($n = 11$). ***$P < 0.01$, ****$P < 0.001$, n.s., not significant. (D) The representative swimming paths and paths heat map of mice in MWM test. The significant differences of each group were compared with group AD.

changes. The results showed the level of the phosphorylated TAU protein in the administration groups was significantly lower than that in AD and free rapamycin groups, which was comparable to the healthy group (Fig. 6A and B). We also studied the Aβ plaques in the hippocampus and cerebral cortex of AD mice brain by immunostaining. As shown in Fig. 6C and 0.36% of Aβ plaques were distributed in the brain of healthy mice. And in AD mice, this value increased more than 10 times to 3.95%. Fortunately, after treatment of nanoparticles, the distribution of Aβ plaques in the brain was greatly reduced, almost close to the level of normal mice. Similar results were obtained in immunohistochemical staining of Aβ plaques (Fig. 6D and Supporting Information Fig. S9A). There have been numerous studies reported in previous studies that Aβ plaques and TAU protein are overexpressed in AD mice[10,43,44]. Interestingly, after receiving R@(ox-PLGA)-KcD treatment, the burden of Aβ plaques and TAU protein decreased significantly. Given these results, we could find that the R@(ox-PLGA)-KcD could promote autophagy and accelerate the degradation and elimination of toxic protein like Aβ plaques and TAU protein in brain.

3.7. *Evaluating neuroprotective effect of nanoparticles*

In addition to toxic protein damage, excessive oxidative stress and high levels of inflammatory response are also important factors that threaten the brain. Research suggested that rapamycin could alleviate oxidative stress and down regulate the levels of inflammatory factors[24]. Furthermore, the ROS responsive bond in nanoparticles would consume a certain amount of ROS in the process of its rupture, which could further alleviate oxidative stress. The ROS levels in the brain of AD transgenic mice were measured at the end of the treatment period. According to the results, the relative ROS level in the brains of mice treated with PBS and free rapamycin were significantly higher than that of healthy mice, while it was dramatically lowered in those receiving R@(ox-PLGA)-KcD treatment (Fig. 7A). Enzyme–linked immunosorbent assay (ELISA) was utilized to detect the level of inflammatory–related factors such as IFN-γ, TNF-α and IL-10 in the hippocampus of brain and serum. The results showed that the pro–inflammatory factors like IFN-γ, TNF-α were both down–regulated in AD transgenic mice treated with R@(ox-PLGA)-KcD, and anti–inflammatory factor IL-10 was up-regulated (Fig. 7B and C and Supporting Information Fig. S9B). This illustrated the R@(ox-PLGA)-KcD could reduce excessive ROS and down–regulate inflammatory factors levels in AD mice, thereby normalizing the lesion microenvironment.

Accordingly, the H&E and Nissl staining in AD mice brain were employed to evaluate the neuronal damage, which could reflect neurotoxicity. In particular, the CA1 and CA3 regions of the hippocampus were often used for memory studies[45]. In Nissl staining, we could observe nuclear stain to deepen, cell body shrinkage, divergence of cell and Nissl bodies decrease in the CA1 and CA3 regions of the hippocampus of mice treated with PBS and free rapamycin, but not in healthy mice and those treated with R@(ox-PLGA)-KcD (Fig. 7D and Supporting Information Fig. S10A). The H&E staining results were consistent with the Nissl staining results (Fig. 7E and Supporting Information Fig.

Please cite this article as: Lei Ting et al., A nanocleaner specifically penetrates the blood–brain barrier at lesions to clean toxic proteins and regulate inflammation in Alzheimer's disease, Acta Pharmaceutica Sinica B, https://doi.org/10.1016/j.apsb.2021.04.022

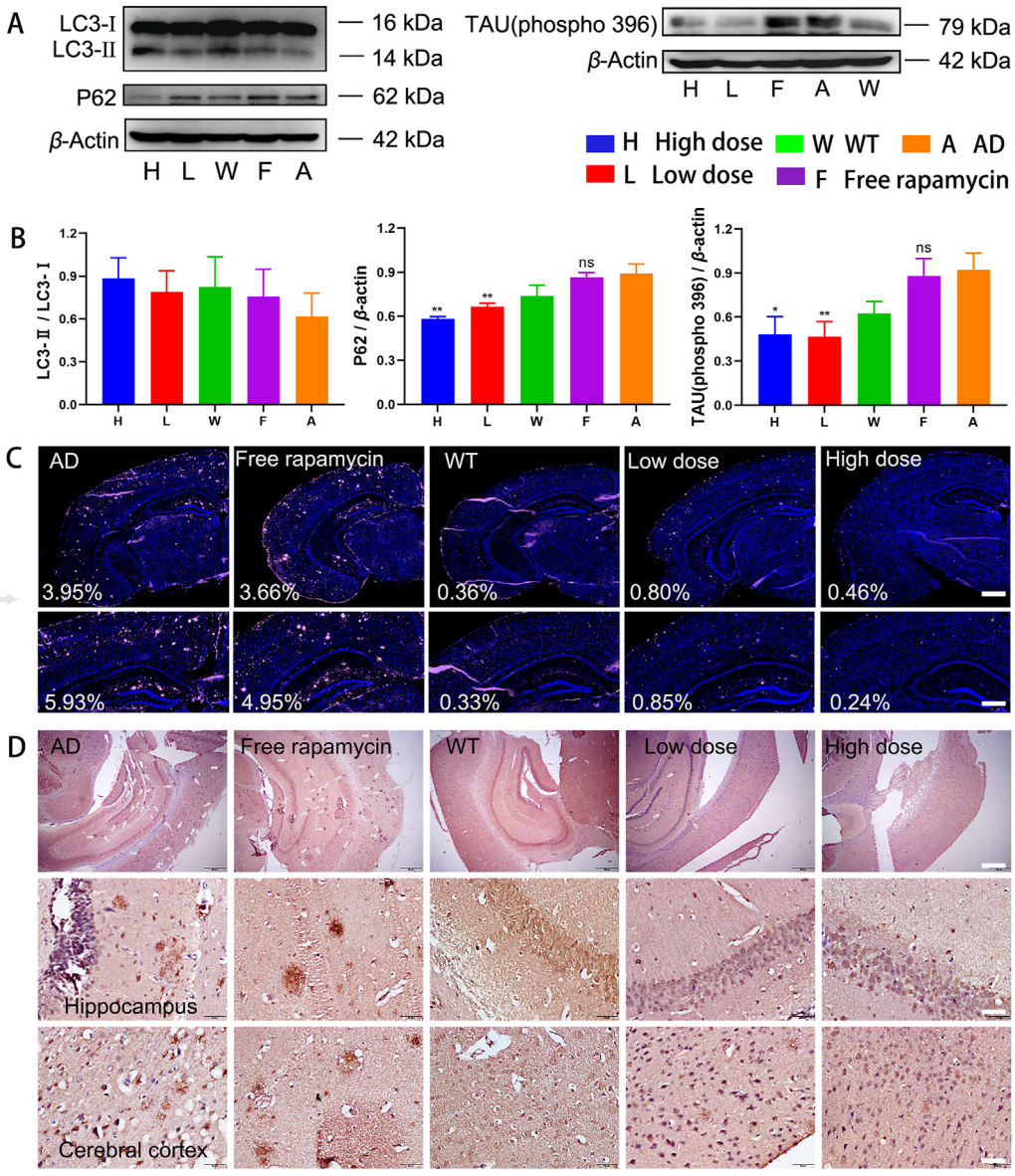

Figure 6 Evaluation of inducing autophagy and cleaning toxic protein *in vivo*. (A) Western blot of LC3-I, LC3-II, p62 and TAU results. (B) The corresponding quantified results from A. Data are presented as mean ± SD ($n = 3$). *$P < 0.05$, **$P < 0.01$, n.s., not significant. The significant differences of each group were compared with group AD. (C) Immunofluorescence staining of Aβ plaques (pink: Aβ; blue: DAPI) in the transgenic mice brain. The first line: Scale bar = 500 μm, the last line: Scale bar = 200 μm. (D) Immunohistochemical staining of Aβ plaques in the brain of AD transgenic mice treated with different formulations. White arrows pointed to Aβ plaques. The first line: Scale bar = 200 μm, the last two lines: Scale bar = 20 μm.

S10B). From these results, we could see that R@(ox-PLGA)-KcD had outstanding effect in protecting nerve cells.

3.8. *Evaluation of toxicity in vivo*

The toxicity of nanoparticles *in vivo* was mainly evaluated by organ H&E staining and weight monitoring. There were no observed pathological differences in different treatment groups (Supporting Information Fig. S11A). The body weight changes of AD mice were not significantly during the treatment (Supporting Information Fig. S11B). These results indicated that the nanoparticles had good biocompatibility and possessed potential clinical application value.

4. Discussion and conclusions

It is urgent to find therapies and delivery methods that slow or reverse the progression of AD. In this study, we successfully designed an accurate targeting nanoparticle [R@(ox-PLGA)-KcD], which could not only specifically capture Aβ, but also mediate the disordered lesion microenvironment for further treatment. The DAG peptide connected to nanoparticles with an acid–sensitive bond could detach from the nanoparticles after specifically targeting the BBB in AD lesions, facilitating the transcytosis of the nanoparticles into the brain parenchyma. KLVFF peptide modified on nanoparticles with short-chain PEG

Please cite this article as: Lei Ting et al., A nanocleaner specifically penetrates the blood–brain barrier at lesions to clean toxic proteins and regulate inflammation in Alzheimer's disease, Acta Pharmaceutica Sinica B, https://doi.org/10.1016/j.apsb.2021.04.022

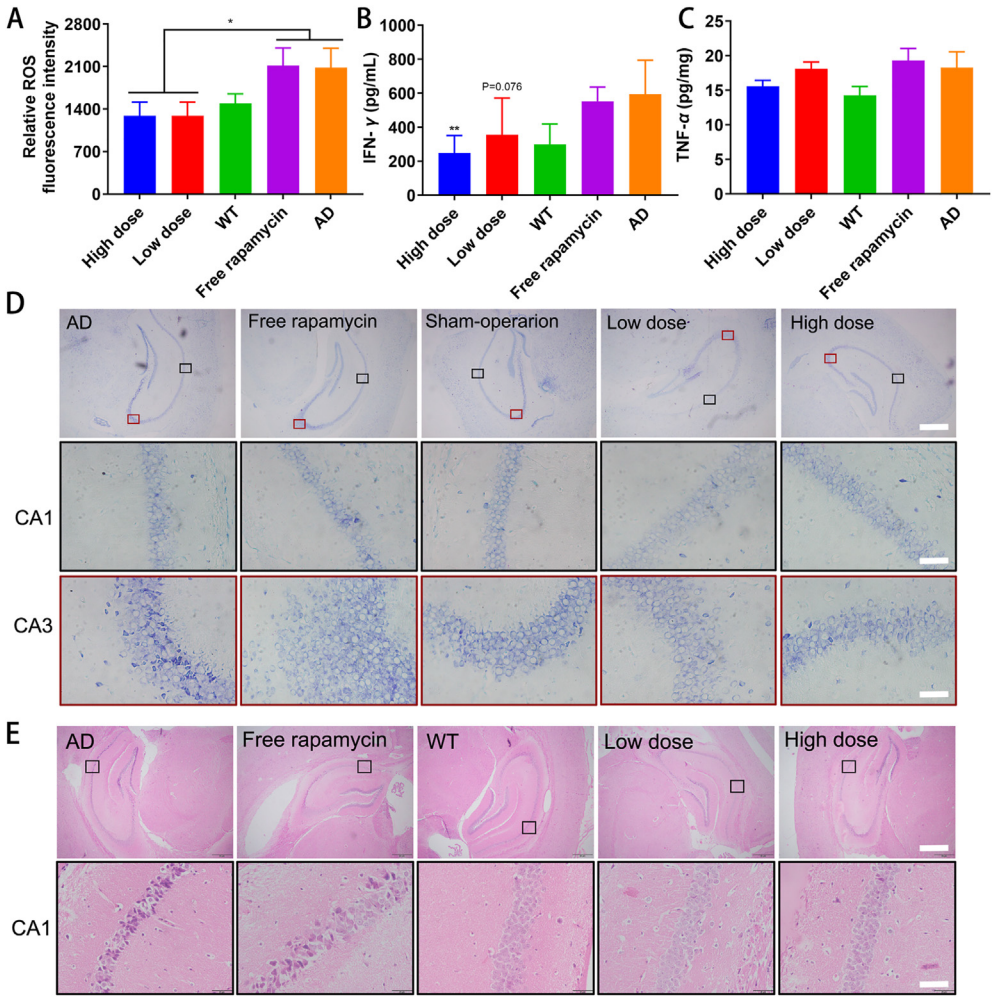

Figure 7 Evaluation of neuroprotective effects and toxicity *in vivo*. (A) Relative ROS level in the hippocampus of AD transgenic mice brain. Data are presented as mean ± SD ($n = 3$). *$P < 0.01$. (B) The level of inflammatory factor IFN-γ in the serum of AD transgenic mice. Data are presented as mean ± SD ($n = 6$). **$P < 0.01$. (C) The level of inflammatory factor TNF-α in the brain of AD transgenic mice. Data are presented as mean ± SD ($n = 3$). The significant differences of each group were compared with group AD. (D) The representative Nissl staining of AD mice (Aβ-injected mice) treated with different formulations. The black box shows the hippocampal CA1 area, the red shows CA3 area. The first line: Scale bar = 200 μm, the last two lines: Scale bar = 20 μm. (E) The H&E staining of AD transgenic mice treated with different formulations. The black box shows the hippocampal CA1 area. The first line: Scale bar = 200 μm, the last line: Scale bar = 20 μm.

was exposed to capture and carry Aβ into microglia after losing long-chain PEG conjugated DAG. In addition, rapamycin released responsively at the lesion sites played a coordinated role to normalize the lesion microenvironment.

In the development of delivery vector for AD, brain-targeting peptides were widely used due to low immunogenicity and high safety[46,47]. For example, BBB shuttle peptide CRT modified on nanoparticles improved the brain targeting of nanoparticles[27]. However, the lack of specificity of this kind of brain-targeting peptide caused the widespread distribution of nanoparticles in the brain, which reduced the accumulation of nanoparticles in lesions as well as brought side effects to normal brain tissue. Likewise, the use of α-D-mannopyranoside as the targeting molecule also faced the above problems[48]. Recent years, some cascade targeting strategies were designed, which first targeted BBB through the primary targeting molecule, and then targeted the lesion sites through the secondary targeting molecule[29,49]. Actually, there is still a long way to reach the lesions after crossing the BBB. These kinds of strategies do not fundamentally solve the non-selectivity of primary targets. Herein, we optimized the previous indiscriminate targeting through a cyclic peptide DAG, which could specifically home to neurovascular unit endothelial cells and reactive astrocytes in AD lesions. From *in vitro* and *in vivo* targeting studies, we found the fluorescence intensity of nanoparticles modified with DAG peptide was mainly concentrated in the injection area of Aβ, confirming that nanoparticles possessed specific brain targeting with the support of DAG.

However, it should be noted that finding a specific brain targeting peptide does not necessarily lead to successful brain accumulation. The reason is that the receptor-mediated transcytosis of brain-targeted peptides still limited by multiple factors in the process of crossing the BBB. In order to improve the binding with BBB, many high-affinity brain-targeting peptides were chose to modify on nanoparticles[48,50]. But in this way, these nanoparticles were prone to trap in endo/lysosomes, causing undesirable transcytosis efficiency. It was reported low-affinity molecules could better mediate transcytosis across BBB, while they were generally required for high concentration to ensure adequate uptake[51]. For balancing the

Please cite this article as: Lei Ting et al., A nanocleaner specifically penetrates the blood–brain barrier at lesions to clean toxic proteins and regulate inflammation in Alzheimer's disease, Acta Pharmaceutica Sinica B, https://doi.org/10.1016/j.apsb.2021.04.022

binding and transcytosis to maximize the benefits, acid-breakage targeting peptides were proposed to enhance the penetration of BBB. After being endocytosed into endo/lysosome, the acid–cleavable brain-targeting peptides could detach from nanoparticles in response to the acid environment, enabling the nanoparticles separate from corresponding receptors to enter brain parenchyma[52]. In our previous research, we also used high-affinity targeting peptides connected with acid–sensitive bond to increase penetration, and achieved excellent brain targeting effects[28,33]. Whereas, there are rarely such reported on specific targeting molecules of BBB in AD lesions. Thus, we equipped the DAG peptide, which could specifically target BBB at AD lesions, with endosome detachable property through acid–sensitive bond. Similarly, the data provided by the *in vitro* BBB model experiment was consistent with the previous studies[28,33]. The nanoparticles modified with acid-cleavable DAG exhibited about two times higher penetration depth than those with acid–uncleavable DAG, indicating the acid–cleavable DAG made the nanoparticles easier to penetrate through the BBB.

For AD treatment, many studies have confirmed that it is not enough to focus on reducing Aβ or TAU protein phosphorylation alone[7,8]. Due to the increasingly prominent role of microglia dysfunction in AD, many current studies have included the restoration of microglial homeostasis into the consideration of therapeutic strategies. An autophagy promoting peptide beclin-1 was delivered to the brain to induce autophagy of microglia to degrade Aβ[21]. But the over activation of microglia in AD lesions not only affects the degradation of toxic proteins due to damaged autophagy system, but also releases a large number of inflammatory factors, ROS and so on, which accelerates the neuronal necrosis[53]. Herein, we co-delivered the Aβ-capturing peptide (KLVFF) and mTOR inhibitor rapamycin. KLVFF peptide could help extracellular Aβ that was not easily absorbed to be endocytosed by microglia. For one thing, it reduced the Aβ-mediated neurotoxicity, for another, it created conditions for microglia to degrade Aβ through intracellular autophagy. The release of rapamycin could restore the damaged autophagy function of microglia, thereby synergizing with KLVFF to reduce Aβ deposition. Not only such, rapamycin could also reverse inflammation condition and alleviate oxidative damage to modulate abnormal microenvironment. Biological sample analysis of AD transgenic mice after treatment provided strong evidence for remarkable anti-AD therapeutic effect of this combinatorial strategy. Collectively, we provide a multi-pronged strategy for delivering therapeutic agents efficiently to AD lesions, which could be regarded as a promising strategy in the development of novel AD treatments.

Acknowledgments

The work was supported by National Natural Science Foundation of China (No. 81872806), 111 Project (No. B18035, China) and the Fundamental of Research Funds for the Central University (China). Macau Science and Technology Development Foundation (No. FDCT 0009/2019/A, China). The authors also acknowledge the technical support from Chenghui Li in Analytical & Testing Center, Sichuan University, China.

Author contributions

Huile Gao, Xiaolin Wang and Ting Lei conceived the project. Ting Lei, Zhihang Yang, Xue Xia, Yuxiu Chen, Xiaotong Yang, Rou Xie and Fan Tong performed experiments. Ting Lei and Huile Gao analyzed the data and wrote the manuscript. All of the authors have read and approved the final manuscript.

Conflicts of interest

The authors declare no conflicts of interest.

Appendix A. Supporting information

Supporting data to this article can be found online at https://doi.org/10.1016/j.apsb.2021.04.022.

References

1. Gaugler J, James B, Johnson T, Marin A, Weuve J. 2019 Alzheimer's disease facts and figures. *Alzheimers Dement* 2019;**15**:321−87.
2. Prakash A, Dhaliwal GK, Kumar P, Majeed ABA. Brain biometals and Alzheimer's disease—boon or bane?. *Int J Neurosci* 2017;**127**:10.
3. Bartus RT, Dean RL, Beer B, Lippa AS. The cholinergic hypothesis of geriatric memory dysfunction. *Science* 1982;**217**:408−14.
4. Han JY, Besser LM, Xiong CJ, Kukull WA, Morris JC. Cholinesterase inhibitors may not benefit mild cognitive impairment and mild Alzheimer disease dementia. *Alzheimer Dis Assoc Disord* 2019;**33**:87−94.
5. Rockwood K, Howlett SE, Hoffman D, Schindler R, Mitnitski A. Clinical meaningfulness of Alzheimer's disease assessment scale–cognitive subscale change in relation to goal attainment in patients on cholinesterase inhibitors. *Alzheimers Dement* 2017;**13**:1098−106.
6. Sharma K. Cholinesterase inhibitors as Alzheimer's therapeutics. *Mol Med Rep* 2019;**20**:1479−87.
7. Long JM, Holtzman DM. Alzheimer disease: an update on pathobiology and treatment strategies. *Cell* 2019;**179**:312−39.
8. Wen MM, El–Salamouni NS, El–Refaie WM, Hazzah HA, Ali MM, Hanafy AS, et al. Nanotechnology–based drug delivery systems for Alzheimer's disease management: technical, industrial, and clinical challenges. *J Control Release* 2017;**245**:95−107.
9. He Z, Guo JL, Mcbride JD, Narasimhan S, Kim H, Changolkar L, et al. Amyloid–β plaques enhance Alzheimer's brain TAU–seeded pathologies by facilitating neuritic plaque TAU aggregation. *Nat Med* 2017;**24**:29−38.
10. Gjoneska E, Pfenning AR, Mathys H, Quon G, Kundaje A, Tsai LH, et al. Conserved epigenomic signals in mice and humans reveal immune basis of Alzheimer's disease. *Nature* 2015;**518**:365−9.
11. Deng ZQ, Purtell K, Lachance V, Wold MS, Chen S, Yue ZY. Autophagy receptors and neurodegenerative diseases. *Trends Cell Biol* 2017;**27**:491−504.
12. Meco AD, Curtis ME, Lauretti E, Praticò D. Autophagy dysfunction in Alzheimer's disease:mechanistic insights and new therapeutic opportunities. *Biol Psychiatr* 2020;**87**:797−807.
13. Zhao Y, Zhang YD, Zhang J, Zhang XJ, Yang GF. Molecular mechanism of autophagy: its role in the therapy of Alzheimer's disease. *Curr Neuropharmacol* 2020;**18**:720−39.
14. Butterfield DA, Mattson MP. Apolipoprotein E and oxidative stress in brain with relevance to Alzheimer's disease. *Neurobiol Dis* 2020;**138**:104795.
15. Wang P, Wang F, Ni L, Wu PF, Chen JG. Targeting redox–altered plasticity to reactivate synaptic function: a novel therapeutic strategy for cognitive disorder. *Acta Pharm Sin B* 2020;**11**:599−608.
16. Birch AM, Katsouri L, Sastre M. Modulation of inflammation in transgenic models of Alzheimer's disease. *J Neuroinflammation* 2014;**11**:25.
17. Irwin MR, Vitiello MV. Implications of sleep disturbance and inflammation for Alzheimer's disease dementia. *Lancet Neurol* 2019;**18**:296−306.
18. Zeng HH, Qi YJ, Zhang ZY, Liu CT, Peng WJ, Zhang Y. Nanomaterials toward the treatment of Alzheimer's disease: recent

advances and future trends. *Chin Chem Lett* 2021. Available from: https://doi.org/10.1016/j.cclet.2021.01.014.
19. Chafekar SM, Malda H, Merkx M, Meijer EW, Viertl D, Lashuel HA, et al. Branched KLVFF tetramers strongly potentiate inhibition of β–amyloid aggregation. *Chembiochem* 2007;**8**:1857−64.
20. Liu DC, Fu DJ, Zhang LB, Sun LM. Detection of amyloid–beta by Fmoc–KLVFF self–assembled fluorescent nanoparticles for Alzheimer's disease diagnosis. *Chin Chem Lett* 2020;**32**:1066−70.
21. Luo Q, Lin YX, Yang PP, Wang Y, Qi GB, Qiao ZY, et al. A self–destructive nanosweeper that captures and clears amyloid β–peptides. *Nat Commun* 2018;**9**:1802.
22. Sarkar S. Role of autophagy in neurodegenerative diseases. *Curr Sci* 2011;**101**:514−9.
23. Cai ZY, Zhao B, Li KS, Zhang LQ, Li CH, Quazi SH, et al. Mammalian target of rapamycin: a valid therapeutic target through the autophagy pathway for alzheimer's disease?. *J Neurosci Res* 2012;**90**:1105−18.
24. Cai ZY, Yan LJ. Rapamycin, autophagy, and Alzheimer's disease. *J Biochem Pharmacol Res* 2013;**1**:84−90.
25. Liu YD, Su Y, Wang JJ, Sun SG, Wang T, Qiao X, et al. Rapamycin decreases TAU phosphorylation at Ser 214 through regulation of cAMP–dependent kinase. *Neurochem Int* 2013;**62**:458−67.
26. Liu RY, Yang J, Liu LY, Lu ZG, Zhang X. An "amyloid–β cleaner" for the treatment of Alzheimer's disease by normalizing microglial dysfunction. *Adv Sci* 2020;**7**:1901555.
27. Zhang L, Liu XG, Liu DQ, Yu XL, Zhang LX, Zhu J, et al. A conditionally releasable "do not eat me" CD47 signal facilitates microglia–targeted drug delivery for the treatment of Alzheimer's disease. *Adv Funct Mater* 2020;**30**:1910691.
28. Cai LL, Yang CY, Jia WF, Liu YW, Xie R, Lei T, et al. Endo/lysosome–escapable delivery depot for improving BBB transcytosis and neuron targeted therapy of Alzheimer's disease. *Adv Funct Mater* 2020;**30**:1909999.
29. Gao HL, Pan SQ, Yang Z, Cao SJ, Chen C, Jiang XG, et al. A cascade targeting strategy for brain neuroglial cells employing nanoparticles modified with angiopep–2 peptide and EGFP–EGF1 protein. *Biomaterials* 2011;**32**:8669−75.
30. Liang H, Chen J. Evolution of blood−brain barrier in brain diseases and related systemic nanoscale brain–targeting drug delivery strategies. *Acta Pharm Sin B* 2020. Available from: https://doi.org/10.1016/j.apsb.2020.11.023.
31. Maussang D, Rip J, Van KJ, Den HAV, Der PSMAV, Der BBV, et al. Glutathione conjugation dose–dependently increases brain–specific liposomal drug delivery *in vitro* and *in vivo*. *Drug Discov Today Technol* 2016;**20**:59−69.
32. Patel MM, Patel BM. Crossing the blood−brain barrier: recent advances in drug delivery to the brain. *CNS Drugs* 2017;**31**:109−33.
33. Ruan SB, Qin L, Xiao W, Hu C, Zhou Y, Wang RR, et al. Acid–responsive transferrin dissociation and GLUT mediated exocytosis for increased blood−brain barrier transcytosis and programmed glioma targeting delivery. *Adv Funct Mater* 2018;**28**:1802227.
34. Mann AP, Scodeller P, Hussain S, Braun GB, Mölder T, Kadri T, et al. Identification of a peptide recognizing cerebrovascular changes in mouse models of Alzheimer's disease. *Nat Commun* 2017;**8**:1403.
35. Wiley DT, Webster P, Gale A, Davis ME. Transcytosis and brain uptake of transferrin–containing nanoparticles by tuning avidity to transferrin receptor. *Proc Natl Acad Sci U S A* 2013;**110**:8662−7.
36. Ruan SB, Qin L, Xiao W, Hu C, Zhou Y, Wang RR, et al. Acid–responsive transferrin dissociation and GLUT mediated exocytosis for increased blood–brain barrier transcytosis and programmed glioma targeting delivery. *Adv Funct Mater* 2018;**28**:1802227.
37. Yang XT, Chen XC, Lei T, Qin L, Zhou Y, Hu C. The construction of *in vitro* nasal cavity–mimic M–cell model, design of M cell–targeting nanoparticles and evaluation of mucosal vaccination by nasal administration. *Acta Pharm Sin B* 2020;**10**:1094−105.
38. Zheng XY, Pang XY, Yang P, Wan X, Wei Y, Guo Q, et al. A hybrid siRNA delivery complex for enhanced brain penetration and precise amyloid plaque targeting in Alzheimer's disease mice. *Acta Biomater* 2017;**49**:388−401.
39. Huang F, Wang JZ, Qu AT, Shen LL, Liu JJ, Liu JF, et al. Maintenance of amyloid β peptide homeostasis by artificial chaperones based on mixed–shell polymeric micelles. *Angew Chem* 2014;**53**:8985−90.
40. Hideyuki A, Takeshi K, Takashi K, Tatsuya N, Naoaki S, Norihiko T. Blood–brain barrier formation of grafted human umbilical vein endothelial cells in athymic mouse brain. *Brain Res* 2000;**858**:172−6.
41. Verkhratsky A, Olabarria M, Noristani HN, Yeh CY, Rodriguez JJ. Astrocytes in Alzheimer's disease. *Neurotherapeutics* 2010;**7**:399−412.
42. Salter MW, Beggs S. Sublime microglia: expanding roles for the guardians of the CNS. *Cell* 2014;**158**:15−24.
43. He ZH, Guo JL, Mcbride JD, Narasimhan S, Kim H, Changolkar L, et al. Amyloid–beta plaques enhance Alzheimer's brain TAU–seeded pathologies by facilitating neuritic plaque TAU aggregation. *Nat Med* 2018;**24**:29−38.
44. James BD, Bennett DA. Causes and patterns of dementia: an update in the era of redefining Alzheimer's disease. *Annu Rev Publ Health* 2019;**40**:65−84.
45. Newrzella D, Pahlavan PS, Kruger C, Boehm C, Sorgenfrei O, Schrock H, et al. The functional genome of CA1 and CA3 neurons under native conditions and in response to ischemia. *BMC Genom* 2007;**8**:370.
46. Sáncheznavarro M, Giralt E, Teixidó M. Blood−brain barrier peptide shuttles. *Curr Opin Chem Biol* 2017;**38**:134.
47. Wu LP, Ahmadvand D, Su JN, Hall A, Tan XL, Farhangrazi ZS, et al. Crossing the blood–brain−barrier with nanoligand drug carriers self−assembled from a phage display peptide. *Nat Commun* 2019;**10**:4635.
48. Liu RY, Yang J, Liu LY, Lu ZG, Shi ZY, Ji WH, et al. An "amyloid−beta cleaner" for the treatment of Alzheimer's disease by normalizing microglial dysfunction. *Adv Sci* 2020;**7**:1901555.
49. Wang PZ, Zheng XY, Guo Q, Yang P, Jiang XG. Systemic delivery of BACE1 siRNA through neuron−targeted nanocomplexes for treatment of Alzheimer's disease. *J Control Release* 2018;**279**:220−33.
50. Lu ZG, Li Y, Shi YJ, Li YH, Xiao ZB, Zhang X. Traceable nanoparticles with spatiotemporally controlled release ability for synergistic glioblastoma multiforme treatment. *Adv Funct Mater* 2017;**27**:1703961−7.
51. Yu YJ, Zhang Y, Kenrick M, Hoyte K, Luk W, Lu Y, et al. Boosting brain uptake of a therapeutic antibody by reducing its affinity for a transcytosis target. *Sci Transl Med* 2011;**3**:84ra44.
52. Clark AJ, Davis ME. Increased brain uptake of targeted nanoparticles by adding an acid−cleavable linkage between transferrin and the nanoparticle core. *Proc Natl Acad Sci U S A* 2015;**112**:12486−91.
53. Kerenshaul H, Spinrad A, Weiner A, Matcovitchnatan O, Dvirszternfeld R, Ulland TK, et al. A unique microglia type associated with restricting development of Alzheimer's disease. *Cell* 2017;**169**:1276−90.

Please cite this article as: Lei Ting et al., A nanocleaner specifically penetrates the blood–brain barrier at lesions to clean toxic proteins and regulate inflammation in Alzheimer's disease, Acta Pharmaceutica Sinica B, https://doi.org/10.1016/j.apsb.2021.04.022